Bull Earthquake Eng (2010) 8:257–282
DOI 10.1007/s10518-009-9128-3

ORIGINAL RESEARCH PAPER

Equivalent linear substructure approximation of soil–foundation–structure interaction: model presentation and validation

Dimitris Pitilakis · Didier Clouteau

Received: 4 November 2008 / Accepted: 24 May 2009 / Published online: 7 June 2009

Abstract An equivalent linear substructure approximation of the soil–foundation–structure interaction is proposed in this paper. Based on the inherent linearity of the approach, the solution of the structural and the soil domain is obtained simultaneously, incorporating the effects of the primary and secondary soil nonlinearities. The proposed approximation is established theoretically and then validated against centrifuge benchmark soil–foundation–structure interaction tests. The equivalent linear substructure approximation is proved to simulate efficiently the effects of the nonlinear soil behavior on the soil–foundation–structure system under a strong earthquake ground motion.

Keywords Soil–foundation–structure interaction · Substructure · Equivalent linear · Centrifuge

1 Introduction

In the soil–foundation–structure interaction (SFSI) there are two types of nonlinearities that might arise under strong ground shaking (Roesset and Tassoulas 1982). The first type is the primary nonlinearity, stemming from the seismic wave induced deformations in the free-field soil. This nonlinearity arises from the nonlinear behavior of the soil as a material, typically associated with a reduction in the shear strain modulus and an increase in the hysteretic dissipation of energy. This type of nonlinearity, which becomes more pronounced with increasing level of ground shaking and soil deformation, is typically addressed in engineering and research practice and well established methods exist for its consideration in the dynamic soil–foundation–structure interaction (SFSI) analyses. The secondary nonlinearity

D. Pitilakis (✉)
Department of Civil Engineering, Aristotle University of Thessaloniki,
P.O. Box 424, 54124 Thessaloniki, Greece
e-mail: dpitilak@civil.auth.gr

D. Clouteau
Ecole Centrale Paris, Grande Voie des Vignes, 92295 Chatenay-Malabry, France

is the one arising from the stresses induced back in the soil from the oscillation of the structure. Secondary nonlinearity may be important in the design of underground structures and lifelines. Nevertheless, according to Mylonakis et al. (2006) no simple realistic solution has been reported in the literature for this latter type of nonlinearity.

Two basic methods and various alternates exist for the analysis of the SFSI phenomenon. In the direct method the entire soil–foundation–structure system is analyzed in a single step, usually by a finite element model. The direct method accepts material and geometrical nonlinearity, but for a three-dimensional nonlinear dynamic analysis it is still very expensive in computational terms and has inherent problems in satisfying the radiation condition of the wave field towards infinity. The substructure method, on the other hand, is widely used in practice, as it is relatively easy to interpret physically the interaction effects. Many numerical tools exist for the analysis of each subdomain, depending on the complexity of the model, and ranging from simple equivalent mass-spring-dashpot systems (Veletsos and Meek 1974; Bielak 1975; Gazetas 1983; Stewart et al. 1999) to complicated finite element or boundary element models (Bode et al. 2002; Karabalis 2004). The coupling of the interacting subdomains is done through the concept of the foundation dynamic impedance functions (Veletsos and Verbic 1973; Gazetas 1991).

In the current state-of-practice, in order to introduce a true nonlinear behavior for the soil in a SFSI analysis, the only feasible way seems to be through a direct finite element approach. Nevertheless, the computational cost of a three-dimensional full nonlinear dynamic SFSI analysis is prohibitively expensive at present. On the contrary, the substructure method and the simple, yet realistic, concept of the impedance functions, emerge the need for simplified procedures to be developed, able to simulate adequately the effects of the nonlinear behavior of the soil in a soil–foundation–structure interaction analysis. Furthermore, no direct comparison has been reported in the literature between an equivalent linear SFSI approach and experimental results.

In this paper an equivalent linear substructure approximation of the SFSI is proposed. The theoretical background of the procedure is presented, strengthening the succeeding numerical application. The developed numerical method is finally validated against centrifuge benchmark tests. The equivalent linear substructure approximation is proved to simulate efficiently the effects of the nonlinear soil behavior on the soil–foundation–structure system under a strong earthquake ground motion.

2 Model presentation

2.1 Linear formulation of SFSI

2.1.1 Domain definition and notations

Aubry and Clouteau (1992) and Clouteau and Aubry (2003) developed an analytical formulation of the SFSI phenomenon, based on the substructure technique. This approach was integrated in the numerical code MISS3D (Clouteau 2005), performing SFSI analyses in the linear elastic or viscoelastic domain. The definition of the complete system is shown in Fig. 1. It consists of the unbounded domain of the soil Ω_s and the structure Ω_b. The interfaces between the soil and the foundation and between the foundation and the structure are denoted by Σ_{sf} and Σ_{bf}, respectively, while their free boundaries are Γ_{sa} and Γ_{ba}. Each subdomain is assumed to have mass density $\rho_k, k = \mathrm{s}, \mathrm{b}$. The system is subjected to an incident wave field $u_i(x, t)$ propagating from the halfspace, assumed to be unaffected by the presence of

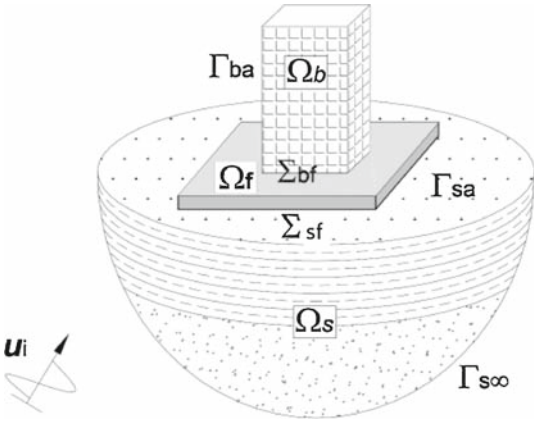

Fig. 1 Definition of the global system

the structure. The displacement field in each subdomain k is denoted by u_k and the traction vector on the interfaces by t_k, oriented by the external normal n. For a vector a:

$$t_{\mathrm{s}}(u_{\mathrm{s}}) \cdot \mathrm{a} \; = \sigma(u_{\mathrm{s}}) : (n \otimes a) \tag{1}$$

where **:** designates the contraction of two tensors, $\cdot$ is the scalar product and $\bigotimes$ is the tensor product of two vectors. The stress tensor Σ_k is associated with the displacement field u_k in each domain. In the soil, the response can be modeled by the equation of Navier, assuming small deformations:

$$\begin{aligned} \sigma\,(u_{\mathrm{s}}) &= \lambda\,[\nabla\,(u_{\mathrm{s}})]\,I_{\mathrm{d}} + 2\mu_{\mathrm{s}}\varepsilon\,(u_{\mathrm{s}}) \\ \varepsilon_{ij} &= \tfrac{1}{2}\left(\partial_i u_j + \partial_j u_i\right) \end{aligned} \tag{2}$$

where ε_{ij} is the strain tensor associated with the displacements u_i and u_j, λ_{s} and μ_{s} are the elastic Lame's coefficients for the soil. Assuming small deformations ε, the displacement vectors u_i and u_{s} verify the Navier equations in the soil:

$$\begin{aligned} \nabla\sigma_{\mathrm{s}}(u_{\mathrm{s}}) &= \rho_{\mathrm{s}}\partial_{\mathrm{tt}}u_{\mathrm{s}} \quad \text{in } \Omega_s \\ \nabla\sigma_{\mathrm{s}}(u_i) &= \rho_{\mathrm{s}}\partial_{\mathrm{tt}}u_i \end{aligned} \tag{3}$$

while u_b satisfies the Navier equations in the structure domain Ω_b:

$$\nabla\sigma_{\mathrm{b}}(u_{\mathrm{b}}) = \rho_{\mathrm{b}}\partial_{\mathrm{tt}}u_{\mathrm{b}} \quad \text{in } \Omega_b \tag{4}$$

2.1.1.1 Boundary conditions The boundary conditions can readily be established. In the soil, the response can be modeled by the equation of Navier, assuming small deformations, and the following boundary conditions must be satisfied:

- Free-field (traction free) conditions on Γ_{sa}
- Continuity of traction and displacements on the soil layer interfaces
- Continuity of displacements on the interface with the foundation

$$u_{\mathrm{s}} = u_{\mathrm{f}} \quad \text{on } \Sigma_{\mathrm{sf}} \tag{5}$$

- Absence of radiation at infinity

$$u_{\mathrm{s}} = u_i \quad \text{on } \Gamma_{\mathrm{s}\infty} \tag{6}$$

In the foundation, the kinematic conditions are as follows:

- Continuity of the displacements on the interface with the soil

$$u_{\mathrm{f}} = u_{\mathrm{s}} \quad \text{on } \Sigma_{\mathrm{sf}} \tag{7}$$

- Continuity of the displacements on the interface with the structure

$$u_{\mathrm{f}} = u_{\mathrm{b}} \quad \text{on } \Sigma_{\mathrm{bf}} \tag{8}$$

In the structure:

- Continuity of the displacements on the interface with the soil on the foundation

$$u_{\mathrm{b}} = u_{\mathrm{s}} \quad \text{on } \Sigma_{\mathrm{bs}} \tag{9}$$

- Traction free conditions on Γ_{ba}

$$t_{\mathrm{b}}(u_{\mathrm{b}}) = 0 \quad \text{on } \Gamma_{\mathrm{ba}} \tag{10}$$

2.1.2 Numerical modeling of the structure

2.1.2.1 Elastodynamic behavior of the structure In the substructure method the structural domain is modeled separately from the soil domain. Numerous software exist for the modeling of the structural response, most conveniently performed with the finite element method (FEM). Evidently, a structure under strong ground shaking may respond in a nonlinear way. Nevertheless, the complexity of the interaction of a nonlinear structure with a nonlinear soil domain reduces the applicability and interest of such an approach. For that reason, herein the structure is considered to respond in the linear domain. Thus, u_{b} verifies the equation:

$$\nabla\sigma_{\mathrm{b}}(u_{\mathrm{b}}) + \rho_{\mathrm{b}}\omega^2 u_{\mathrm{b}} = 0 \quad \text{in } \Omega_{\mathrm{b}} \tag{11}$$

For any virtual displacement $\mathrm{v_b}$, kinematically acceptable, the Principle of the Virtual Works in the domain of the structure can be written as follows:

$$-\int_{\Omega_{\mathrm{b}}} \sigma(u_{\mathrm{b}}) : \varepsilon(v_{\mathrm{b}})\mathrm{d}V - \int_{\Sigma_{\mathrm{sf}}} t_{\mathrm{s}}(u_{\mathrm{s}}) \cdot v_{\mathrm{b}}\mathrm{d}S = -\omega^2 \int_{\Omega_{\mathrm{b}}} \rho_{\mathrm{b}} u_{\mathrm{b}} \cdot v_{\mathrm{b}}\mathrm{d}V \tag{12}$$

where $\sigma(u_b)$ and $\varepsilon(v_b)$ are the real stress field and the virtual strain, respectively, in the structure.

2.1.2.2 Decomposition of the displacement in the structure Assuming the most general case of a rigid foundation, the displacement field in the structure u_{b} can be decomposed in two modal bases: the rigid body modal basis u_{f}, due to the rigid body modes of the foundation, and the flexible modal basis u_{b0} of the structure, due to the elastic structural deformations:

$$u_{\mathrm{b}} = u_{\mathrm{f}} + u_{\mathrm{b0}} \quad \text{in } \Omega_{\mathrm{b}} \tag{13}$$

The rigid body modes of the foundation can be written in the form:

$$u_{\mathrm{f}}(x, \omega) = \sum_{m=1,6} c_m(x, \omega) L_m(x) \quad \forall x \in \Omega_{\mathrm{f}} \tag{14}$$

where $L_m(x)$ are the six rigid body modes and c_m a participation factor depending on the frequency. The first three modes are the translational and the last three the rotational, with the principal coordinate axis system passing from the center of gravity of the foundation. The auxiliary displacement $u_{\mathrm{b}0}$ is decomposed on the flexible modal basis ϕ_{A},

$$u_{\mathrm{b}0}(x,\omega) = \sum_{A\geq 1} q_A(x,\omega)\phi_A(x) \quad \text{in } \Omega_{\mathrm{b}} \tag{15}$$

where ϕ_A are the natural fixed-base modes of the elastic structure of natural frequency ω_A and q_A a participation factor. Then, the total displacement field u_b in the structure will be:

$$u_{\mathrm{b}}(x,\omega) = \sum_{m=1,6} c_m(x,\omega)L_m(x) + \sum_{A\geq 1} q_A(x,\omega)\phi_A(x) \quad \text{in } \Omega_b \tag{16}$$

Introducing Eqs. 12, 16, since the deformation $\varepsilon(L_m)$ for a rigid body movement L_m is zero, the following equation is obtained:

$$\begin{aligned} &-\sum_{A>1} q_A \int_{\Omega_{\mathrm{b}}} \sigma(u_{\mathrm{b}}) : \varepsilon(v_{\mathrm{b}})\mathrm{d}V - \int_{\Sigma_{\mathrm{sf}}} t_{\mathrm{s}}(u_{\mathrm{s}}) \cdot v_{\mathrm{b}}\mathrm{d}S \\ &\quad = -\omega^2 \left[\sum_{m=1,6} c_m \int_{\Omega_{\mathrm{b}}} \rho_{\mathrm{b}} L_m \cdot v_{\mathrm{b}}\mathrm{d}V + \sum_{A>1} q_A \int_{\Omega_{\mathrm{b}}} \rho_{\mathrm{b}}\phi_A \cdot v_{\mathrm{b}}\mathrm{d}V \right] \end{aligned} \tag{17}$$

The kinematically acceptable virtual displacement v_{b} can be written on the basis of the rigid body modes of the foundation, $v_{\mathrm{b}} = L_n$, and Eq. 17 produces the Principle of Virtual Works at the foundation level:

$$-\int_{\Sigma_{\mathrm{sf}}} t_{\mathrm{s}}(u_{\mathrm{s}}) \cdot v_{\mathrm{b}}\mathrm{d}S = -\omega^2 \left[\sum_{m=1,6} c_m \int_{\Omega_{\mathrm{b}}} \rho_{\mathrm{b}} L_m \cdot L_n \mathrm{d}V + \sum_{A\geq 1} q_A \int_{\Omega_{\mathrm{b}}} \rho_{\mathrm{b}}\phi_A \cdot L_n \mathrm{d}V \right] \tag{18}$$

The first term at the right-hand side of Eq. 18 represents the mass matrix M_{b} of the structure, including the foundation mass, assumed to move as a rigid block:

$$[M_{\mathrm{b}}]_{mn} = \int_{\Omega_{\mathrm{b}}} \rho_{\mathrm{b}} L_m L_n \mathrm{d}V \tag{19}$$

The second term of the right-hand side of the equation represents the equivalent added structural mass matrix M_b^* due to the vibration of the flexible structure. For any natural frequency ω_A and mode ϕ_A:

$$\sum_{A\geq 1} q_A \int_{\Omega_{\mathrm{b}}} \rho_{\mathrm{b}}\phi_A \cdot L_n \mathrm{d}V = \sum_{m=1,6} c_m \left[\sum_A \frac{\omega^2}{\omega_A^2 - \omega_A} \int_{\Omega_{\mathrm{b}}} \rho_{\mathrm{b}} L_m \phi_A \mathrm{d}V \int_{\Omega_{\mathrm{b}}} \rho_{\mathrm{b}}\phi_A L_n \mathrm{d}V \right] \tag{20}$$

The added structural mass M_b can therefore be defined as:

$$\left[M_b^*\right]_{mn} = \sum_{A\geq 1} \frac{\omega^2}{\omega_A^2 - \omega_A} \int_{\Omega_{\mathrm{b}}} \rho_{\mathrm{b}} L_m \phi_A \mathrm{d}V \int_{\Omega_{\mathrm{b}}} \rho_{\mathrm{b}}\phi_A L_n \mathrm{d}V \tag{21}$$

Thus,

$$\sum_{A\geq 1} q_A \int_{\Omega_b} \rho_b \phi_A \cdot L_n \mathrm{d}V = \int_{\Omega_b} \rho_b u_{b0} \cdot L_n \mathrm{d}V = \sum_{m=1,6} c_m \left[M_b^*\right]_{mn} \tag{22}$$

In the case where modal damping ζ_A is added in the structural mode ϕ_A, Eq. 22 is written as follows:

$$\left[M_b^*\right]_{mn} = \sum_{A\geq 1} \frac{\omega^2}{\omega_A^2 + 2i\zeta\omega\omega_A - \omega_A} \int_{\Omega_b} \rho_b L_m \phi_A dV \int_{\Omega_b} \rho_b \phi_A L_n \mathrm{d}V \tag{23}$$

Implying that for low frequencies the equivalent structural mass tends towards the static rigid body mass, while for increasing excitation frequency above the fundamental structural frequency the equivalent mass of the vibrating structure will eventually decrease. At the vicinity of the resonance frequency, the term of the added mass for the higher frequency range acts as a dashpot, dissipating energy that enters in the structure.

Equation 18 can be written more consistently in a matrix form:

$$-\int_{\Sigma_{sf}} t_s(u_s) \cdot L_n \mathrm{d}S = -\omega^2 \left[\sum_{m=1,6} c_m \left\{[M_b]_{mn} + \left[M_b^*\right]_{mn}\right\}\right] \tag{24}$$

The sum of the two masses of Eqs. 19 and 23 express the equivalent mass of the structure. The right-hand term of Eq. 24 expresses the effect of the **inertial interaction** on the system response.

2.1.3 Numerical modeling of the soil

2.1.3.1 Elastodynamic behavior of the soil The unbounded domain of the soil is modeled with the Navier elastodynamic equations. Thus, in the frequency domain, in every soil layer the displacement field of the soil u_s verifies the following equation:

$$\nabla\sigma_s(u_s) + \rho_s\omega^2 u_s = 0 \quad \text{in } \Omega_s \tag{25}$$

Moreover, the incident wave field u_i, representing the free-field ground motion in the absence of the structure, has to be compatible with the soil stratigraphy. Subsequently, the following equations have to be assured:

$$\nabla\sigma_s(u_i) + \rho_s\omega^2 u_i = 0 \quad \text{in } \Omega_s \tag{26}$$

$$t_s(u_i) = 0 \quad \text{on } \Gamma_{sa} \tag{27}$$

2.1.3.2 Decomposition of the displacement in the soil On the other hand, in the unbounded soil domain the displacement field u_s is decomposed in two separate fields, the displacement due to the incident wave field u_i and the displacement due to the total diffracted wave field u_d:

$$u_s = u_i + u_d \quad \text{in } \Omega_s \tag{28}$$

The linearity of the problem implies that the boundary conditions imposed to u_s and u_i are satisfied also by u_d:

$$\nabla\sigma_s(u_d) + \rho_s\omega^2 u_d = 0 \quad \text{in } \Omega_s \tag{29}$$

$$t_s(u_d) = 0 \quad \text{on } \Gamma_{sa} \tag{30}$$

The only difference between the boundary conditions imposed on u_d and those of u_s and u_i are on $\Gamma_{s\infty}$ and Σ_{sf}. Following Eqs. 6 and 14, the boundary conditions of u_i and u_s forced by $\Gamma_{s\infty}$ and Σ_{sf}, impose to u_d:

$$\begin{aligned} u_d &= 0 \quad \text{on } \Gamma_{s\infty} \\ u_d &= -u_i + \sum_{m=1,6} c_m L_m \quad \text{on } \Sigma_{sf} \end{aligned} \tag{31}$$

The first equation of Eq. 31 states the radiation condition towards infinity, while the second one suggests a further decomposition of the total displacement u_s in the soil into two secondary displacements. The first component is the displacement due to local diffraction of the incident wave field on the foundation assumed fixed, and the second component is the displacement due to radiation caused by a unitary foundation movement along the mth rigid base mode.

The local diffracted u_{d0} and the radiated u_{dm} displacements verify the Navier's equation in the soil, the free surface conditions on Γ_{sa} and the radiation condition at infinity, notably:

$$\begin{aligned} \nabla\sigma_s(u_{d0}) + \rho_s\omega^2 u_{d0} &= 0 \quad \text{in } \Omega_s \\ u_{d0} &= 0 \quad \text{in } \Omega_b \\ t_s(u_{d0}) &= 0 \quad \text{on } \Gamma_{sa} \\ u_{d0} &= -u_i \quad \text{on } \Sigma_{sf} \end{aligned} \tag{32}$$

and for the radiated wave fields u_{dm}, $m = 1, 6$, in the soil:

$$\begin{aligned} \nabla\sigma_s(u_{dm}) + \rho_s\omega^2 u_{dm} &= 0 \quad \text{in } \Omega_s \\ t_s(u_{dm}) &= 0 \quad \text{on } \Gamma_{sa} \\ u_{dm} &= L_m \quad \text{on } \Sigma_{sf} \end{aligned} \tag{33}$$

Finally, the total displacement field in the soil will be the weighted sum of the incident u_i, the locally diffracted u_{d0} and the radiated u_{dm} wave fields:

$$u_s = u_i + u_{d0} + \sum_{m=1,6} c_m u_{dm} \quad \text{in } \Omega_s \tag{34}$$

The forces imposed on the structure will be:

$$t_s(u_s) = t_s(u_i) + t_s(u_d) \quad \text{on } \Sigma_{sf} \tag{35}$$

or, after Eq. 34,

$$t_s(u_s) = t_s(u_i + u_{d0}) + \sum_{m=1,6} c_m t_s u_{dm} \quad \text{on } \Sigma_{sf} \tag{36}$$

This vector represents the effects of the diffraction of the incident wave field on the foundation, showing clearly the difference between the kinematic response of the free-field and the foundation. It reflects the effects of the earthquake on the foundation and is referred to as **kinematic interaction**. By multiplying Eq. 36 by L_n ($n = 1, 6$) and integrating on Σ_{sf} the following expression is obtained:

$$\int_{\Sigma_{sf}} t_s(u_s) \cdot L_n \mathrm{d}S = \sum_{m=1,6} c_m \int_{\Sigma_{sf}} t_s(u_{dm}) L_n \mathrm{d}S + \int_{\Sigma_{sf}} t_s(u_i + u_{d0}) L_n \mathrm{d}S \tag{37}$$

The first term on the right-hand side of Eq. 37 represents the **generalized dynamic impedance of the soil $\mathbf{K}_s$**

$$[K_s]_{nm} = \int_{\Sigma_{sf}} t_s(u_{dm}) L_n \mathrm{d}S \tag{38}$$

evaluated at the soil-foundation interface Σ_{sf} when subjected to the foundation kinematics, and the second term is the opposite equivalent seismic force F_s

$$[F_s]_n = -\int_{\Sigma_{sf}} t_s(u_i + u_{d0}) L_n \mathrm{d}S \tag{39}$$

introduced at the foundation level by the earthquake ground motion.

The generalized dynamic soil impedance matrix is complex, as in the frequency domain the viscoelastic soil model introduces a complex part in the radiated wave field u_{dm} due to the soil damping. Furthermore, the vibration of the foundation induces additional wave field in the soil, which dissipates energy propagating towards the infinity (radiation condition towards the infinity).

2.1.4 Fundamental equation of SFSI

From Eqs. 37 and 24, the general system of equations of soil-structure interaction can be formulated, having six equations with six unknowns:

$$\left[[K_s] - \omega^2 \left([M_b] + \left[M_b^*\right]\right)\right]\{c\} = \{F_s\} \tag{40}$$

where c is the unknown displacement vector for the six modes of vibration at the center of the foundation.

2.2 Equivalent linear formulation of SFSI

2.2.1 Theoretical approximation

The shear strain level that the soil exhibits during an earthquake is related to the equivalent linear soil properties, namely the shear modulus G and damping ξ, and therefore an iterative procedure is required to ensure that the soil properties used in the analysis are compatible with the level of strain. The shear modulus reduction is reported to vary dramatically due to softening and should be representative of the site conditions (Ghosh and Madabhushi 2007). In a typical equivalent linear analysis, initial estimates of G and ξ are made, usually based on a linear elastic approximation, and then iterative linear analyses are performed, recalculating in each iteration the soil properties based on the estimated level of shear strain response. The procedure ends when the shear modulus and damping converge to an almost constant value. The equivalent linear modeling of the soil behavior is assumed to be well established, at least in the moderate to high frequency range, in the engineering practice and, thus, no further details are needed.

However, the traditional equivalent linear approach for the soil behavior has to be updated in a SFSI analysis, in order to accommodate for the secondary nonlinearities arising from the structural oscillation. Moreover, as the soil behaves in a nonlinear way, the response of the system depends also on the input motion. In contrast with a linear SFSI analysis, in the equivalent linear approximation the characteristics of the input seismic signal

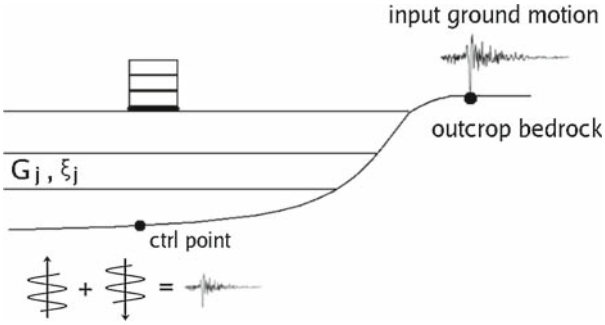

Fig. 2 Deconvolution of the motion from the outcropping bedrock to a control point at the bedrock interface under the soil profile

affect the response of the soil–foundation–structure system and thus, have to be taken into account.

Based on the inherent linearity of the problem, the response of the soil is calculated with an equivalent linear procedure simultaneously with the response of the linear structure. Then, the total response is obtained by linear superposition. The updated iterative procedure operates as follows:

1. Initial estimates are made of the shear modulus $G_{(j)}$ and damping $\xi_{(j)}$ for each soil layer j, as shown in Fig. 2. These initially estimated values correspond to the linear elastic characteristics of the soil in the very low strain range, neglecting the presence of the structure. That is, the initial shear modulus G and damping ξ are estimated for each soil layer j at free-field soil conditions. Moreover, shear modulus reduction G/G_{max} and damping ξ curves are chosen for each soil layer to represent its nonlinear behavior.
2. The earthquake input ground motion is chosen and applied on outcropping bedrock, as shown in Fig. 2.
3. The ground motion at a control point on the interface between the bedrock and the soil profile is evaluated with linear deconvolution of the input ground motion (Fig. 2). The displacement field is calculated in the halfspace using standard one-dimensional wave propagation equations and the equivalent linear properties $G_{(j)}$ and damping $\xi_{(j)}$ of each soil layer j.
4. A linear convolution analysis is performed for the analysis of the soil–foundation–structure system. The estimated values of $G_{(j)}$ and $\xi_{(j)}$ are used to calculate the response in the unbounded soil domain, when subjected to the ground motion defined in the previous step on the control point on the bedrock. Meanwhile, the response of the structure is computed for the same input ground motion, along with the foundation vibration, which creates an additional wave field emanating away from the foundation in the soil.
5. The shear strain time history is calculated in the soil as the inverse Fourier of the shear strain response in the frequency domain. The latter is estimated as a linear superposition of the soil response subjected to two simultaneous phenomena: (a) the incident free-field wave field propagating upwards from the halfspace and (b) the emanating wave field because of the foundation vibration propagating downwards, as shown at the bottom of Fig. 2.
6. The effective shear strain $\gamma_{\text{eff}(j)}$ for each soil layer j is calculated as a portion of the maximum shear strain amplitude $\gamma_{\max(j)}$, usually taken as the 65% of the peak value where j is the soil layer number and i is the iteration number.

$$\gamma^{(i)}_{\text{eff}\,(j)} = R_\gamma \cdot \gamma^{(i)}_{\max\,(j)} \quad \text{where } R_\gamma = 0.65 \tag{41}$$

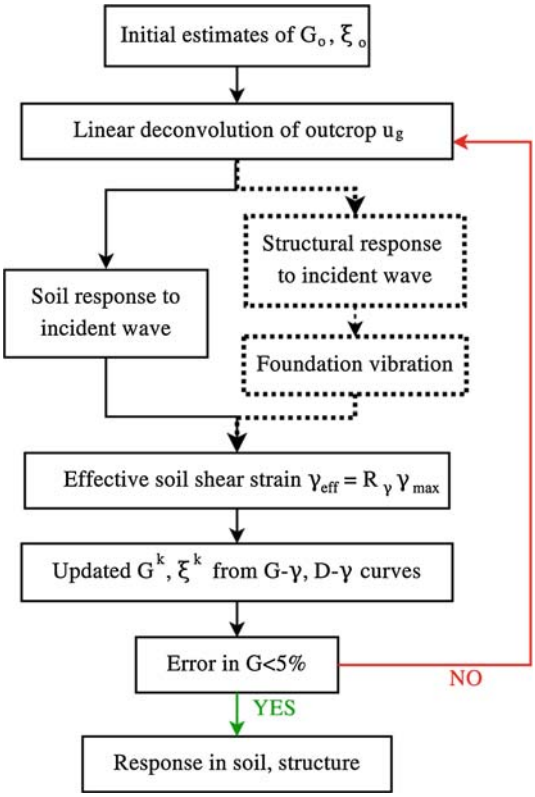

Fig. 3 Updated iterative equivalent linear approach in the substructure method. The novel aspects of the procedure are highlighted by *dashed line*

7. From the estimated effective shear strain $\gamma_{\text{eff}(j)}^{(i)}$ in the jth layer and ith iteration, the new equivalent linear values for the shear modulus $G_{(j)}^{(i+1)}$ and damping $\xi_{(j)}^{(i+1)}$ are calculated with linear interpolation with the provided shear modulus reduction $G/G_{\max}$ and damping ξ curves. These updated values will be used in the next $i+1$ iteration.
8. The new, updated, ground motion at the control point on the bedrock (Fig. 2) is calculated for the next iteration $i+1$. To this end, deconvolution of the input ground motion to the control point is performed, taking into account the updated equivalent linear soil properties $G_{(j)}^{(i+1)}$ and of the $i+1$ iteration.
9. Steps 3 to 8 are repeated until the difference between the computed shear modulus and damping ratio values in two consecutive iterations are lower than a certain predefined limit in all soil layers. Convergence was found to be achieved for not more than five iterations with an error of 5%.

The aforementioned procedure, shown in the flowchart of Fig. 3, is implemented in the numerical code MISS3D-EqL.

2.2.2 Numerical modeling aspects

For the numerical modeling of the problem, assumptions like the following are made in the numerical solution. Detailed description of the numerical procedure can be found in Pitilakis (2006).

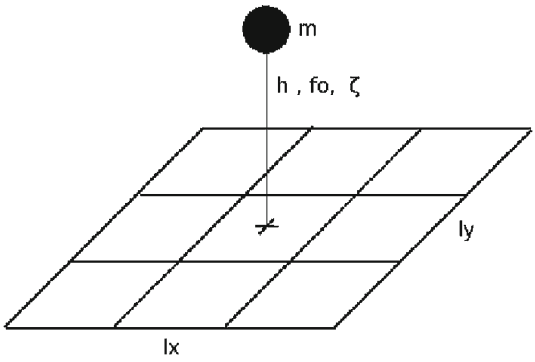

Fig. 4 Structural model considered in the SFSI analyses

- The structure is modeled as an equivalent SDOF with structural mass m, height h, natural frequency f_o and modal damping ζ. The foundation is assumed to be rigid massless rectangular plate resting on the surface of the soil, with dimensions l_x-by-l_y, meshed with quadrilateral finite elements. Even though arbitrary shaped foundations are met in practice, the rectangular foundation is assumed to be a representative generalization. The column of the structure is assumed to be clumped at a point in the geometrical center of the surface foundation, as shown in Fig. 4.
- The soil profile is modeled as infinite horizontal layers of thickness $h_{s(j)}$, with shear wave velocity $V_{s(j)}$, uniform mass density $\rho_{s(j)}$, hysteretic damping ratio $\xi_s(j)$ and Poisson's ratio $\nu_s(j)$. In addition, shear modulus reduction and damping curves are assigned to every soil layer j, expressing its nonlinear behavior. The underlying bedrock is modeled as an infinite soil layer.
- A range of frequencies is chosen, in which the SFSI analysis will be performed. This range is selected based on the Fourier spectrum of the recorded input acceleration time history and the hysteretic damping ratio. The frequency step depends on the irregularity of the Fourier spectrum. Actually, a resonance peak at a frequency f_o and with damping β is of width $2\beta f_o$, and thus a frequency step smaller than the width of the peak is required for its capture. The physical criteria for the frequency sampling can be summarized as:
  - minimum frequency = first non-zero frequency of the signal
  - maximum frequency = maximum frequency of the signal
  - step $df \leq \min(\beta f_o)$
- The displacement time history to be used as input ground motion in the analysis is the product of a baseline correction (Boore et al. 2002) and double integration of the acceleration recorded at outcropping bedrock.

The response in the soil domain is calculated at a series of control points. These control points are chosen in the soil on the vertical axis. In each horizontal soil layer, two control points, $u^{(i)}_{1(j)}$ and $u^{(i)}_{2(j)}$ are placed at a distance of $dh^{(i)}_{(j)}/2$ on both sides of the midpoint of the soil layer, following the vertical direction. The subscript j stands for the soil layer, when i is the iteration number. The distance $dh^{(i)}_{(j)}$ of the control points in the jth soil layer is calculated in every soil layer j,

$$dh^{(i)}_{(j)} \leq \frac{\min V^{(i)}_{s(j)}}{10 f_{\max}} \tag{42}$$

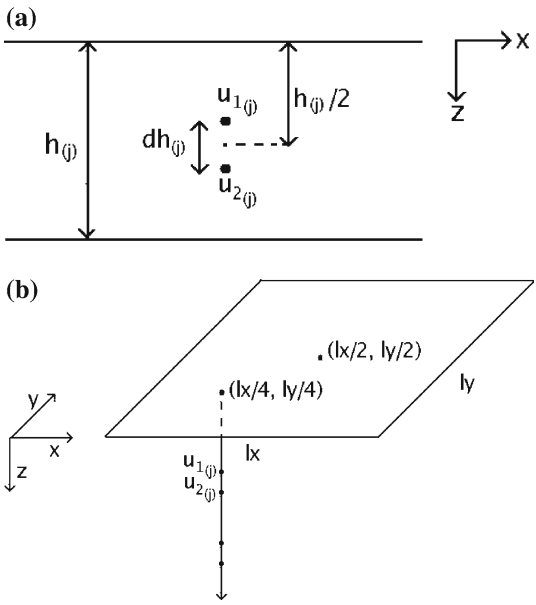

Fig. 5 *Horizontal* and *vertical* position of the control points in the soil, at which the soil response is calculated by MISS3D-EqL (**a**) Selection of control points in the soil in the vertical direction, where the response of the soil is going to be calculated. (**b**) Placement on the control points in the horizontal plane

where $dh_{(j)}^{(i)}$ is the vertical distance of the two control points in the jth soil layer for the ith iteration, $minV_{s(j)}^{(i)}$ is the minimum shear wave velocity of the soil layer j for the ith iteration and $f_{\max}$ is the maximum frequency of the wave field. Figure 5a shows the selection of two control points $u_{1(j)}$ and $u_{2(j)}$ and their relative distance $dh_{(j)}$ in an arbitrary soil layer j. The series of the control points follows the vertical axis that passes at a distance of 1/4 of each side from the corner of the rectangular foundation, as seen in Fig. 5b. The deepest control point is the one on the interface between the soil and the bedrock, used for the linear deconvolution of the motion recorded on outcropping bedrock as well.

The foundation-structure system is modeled as a $7df$ model, with $6df$ expressing the rigid body movement of the solid foundation and the seventh degree of freedom being the horizontal structural displacement of the mass. The participation factors of each one of the seven modes of the foundation-structure system are calculated by standard rigid body dynamics (Chopra 2001).

The analysis of the SFSI problem in each iteration is executed with MISS3D. The soil–foundation–structure system is excited by unitary SV waves, propagating upwards in the vertical direction and polarized in the horizontal direction of the structural degree of freedom. The response in the soil is calculated at the control points chosen as shown in Fig. 5. The response is calculated in the form of an *incident wave* displacement and a *total diffracted wave* displacement, i.e., the locally diffracted wave and the radiated from the foundation in the soil, their sum being the *total wave*:

$$u_{\mathrm{s}} = u_i + u_{\mathrm{d}} \tag{43}$$

From the displacement response to the unitary waves, frequency response functions (FRF) are estimated for the selected frequency range, between the control point on the bedrock and the various control points in the soil. At the same time, the FRF for the foundation-structure degrees of freedom are calculated. In any case, the first iteration of the equivalent linear analysis corresponds to a linear SFSI analysis and the response is saved for reference.

2.3 Discussion on the secondary nonlinearities

The response of the soil may differ significantly from the free-field conditions when the structural vibration is considered, especially for the case of unusually heavy oscillating structures. While most of the studies focus on the effect of the soil secondary nonlinearity on the structural system (Halabian and Naggar 2002), limited interest is shown on the effect of the structural oscillation on the soil response. Besides, the aforementioned effects of heavy oscillating structures on the soil response may be more pronounced in the case of an equivalent linear analysis of the unbounded soil domain. Illustrating these effects, Fig. 6 shows the calculated shear strain time histories in the middle of the uppermost soil layer of a fictitious soil–foundation–structure system, for four different cases. The structure is a water tower, with total oscillating mass of 1000 tones concentrated at a height equal to the foundation width.

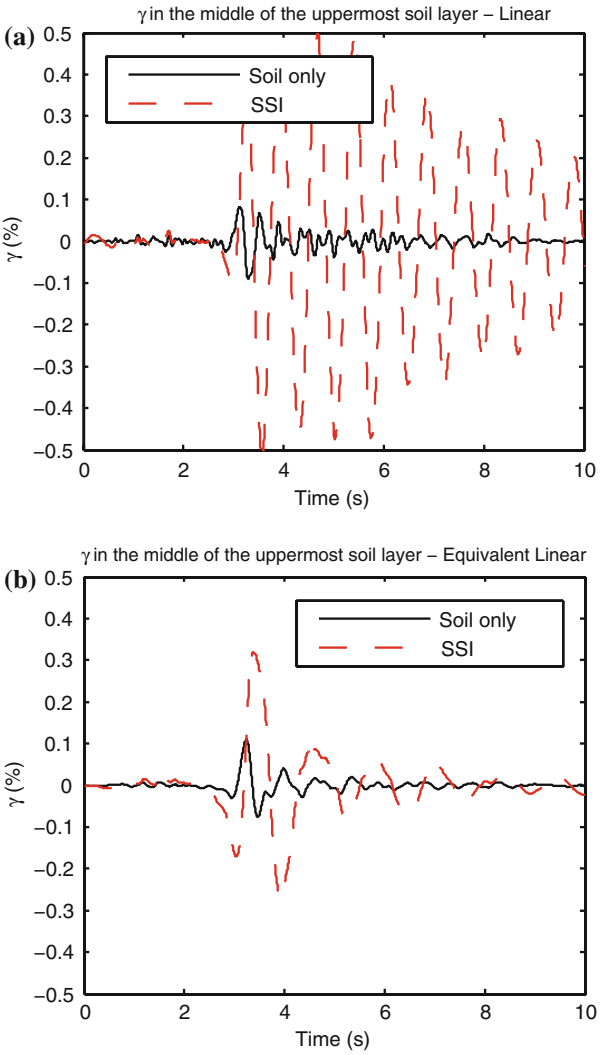

Fig. 6 Shear strain time history in the middle of the uppermost soil layer for linear (**a**) and equivalent linear (**b**) soil behavior, taking into account the existence of the structure and soil nonlinearity. (**a**) Shear strain γ in the middle of the uppermost soil layer for linear soil behavior. (**b**) Shear strain γ in the middle of the uppermost soil layer for equivalent linear soil behavior

The foundation-structure system is founded on the free surface of a soft soil profile. The soil consists of a 6 m thick soft clayey silt layer with $V_s = 130$ m/s, overlying a relatively stiffer clayey soil material with shear wave velocity ranging up to $V_s = 280$ m/s. The shear wave velocity of the upper 30 m of the soil profile is equal to $V_{s30} = 209$ m/s, which classifies the soil to the category C of EC8. The complete system is subjected to the Aegion 1995, Greece strong earthquake record and has the same initial properties in all four cases.

Figure 6a presents the shear strain time histories immediately below the foundation assuming linear soil behavior, for free-field conditions (solid line), and for the complete soil–foundation–structure system (dashed line). Furthermore, Fig. 6b shows the same shear strain time histories but for equivalent linear soil behavior.

It is seen in Fig. 6 that for the same earthquake ground motion and the same initial conditions, the soil response depends on two parameters, the linear or nonlinear soil behavior and the existence or non-existence of the structure.

In this example, considering the effect of the soil nonlinearity, in free-field conditions the equivalent linear approximation produces larger shear strain in the soil. Considering the effect of the existence of the structure, when the complete soil–foundation–structure system is considered the linear approximation produces the largest shear strain under the foundation. This is attributed to the soil nonlinearity, which induces more damping in the system causing lower amplification and more rapid fade out of the response. Moreover, it is seen that the oscillation of the foundation-structure system causes an additional wave field in the soil in the vicinity of the foundation, which in turn increases the shear strain exhibited by the soil. Even though in most typical cases the secondary soil nonlinearities can be ignored compared to the primary nonlinearities (Kausel et al. 1976; Roesset and Tassoulas 1982), in some cases, such as the one presented above, they can be important, especially for lifelines or underground structures. Finally, this SFSI effect is not taken into account in typical dynamic analysis, where the incident wave field in free-field conditions is applied directly as input motion in the foundation, without taking into consideration the SFSI. In this latter case, the response in the soil depends only on the soil conditions and is indifferent to the structural oscillation.

3 Centrifuge testing modeling and validation

While the linear branch of the numerical code was verified against shaking table experimental results Pitilakis et al. (2008), the equivalent linear substructure approximation described above is validated by centrifuge tests. In the context of the European project *NEMISREF*, benchmark centrifuge experiments were conducted in Cambridge University (UCAM), Cambridge, UK. The centrifuge apparatus, situated in the Schofield Center, Cambridge, UK, is documented in Schofield (1980, 1981), Madabhushi et al. (1998) and Brennan and Madabhushi (2002).

The results of the aforementioned experiments were used to validate the accuracy and efficiency of the proposed equivalent linear substructure approximation of the SFSI.

3.1 Experimental apparatus

A SDOF structure was tested on a level, dry, thick sand bed. The centrifuge container is shown in Fig. 7. The rubber layers in between the steel rings around the container have shear modulus of approximately 1.7 MPa. Aluminum sheets with glued sand were placed in the interior, at each side of the container, in order to maintain complementary shear stresses

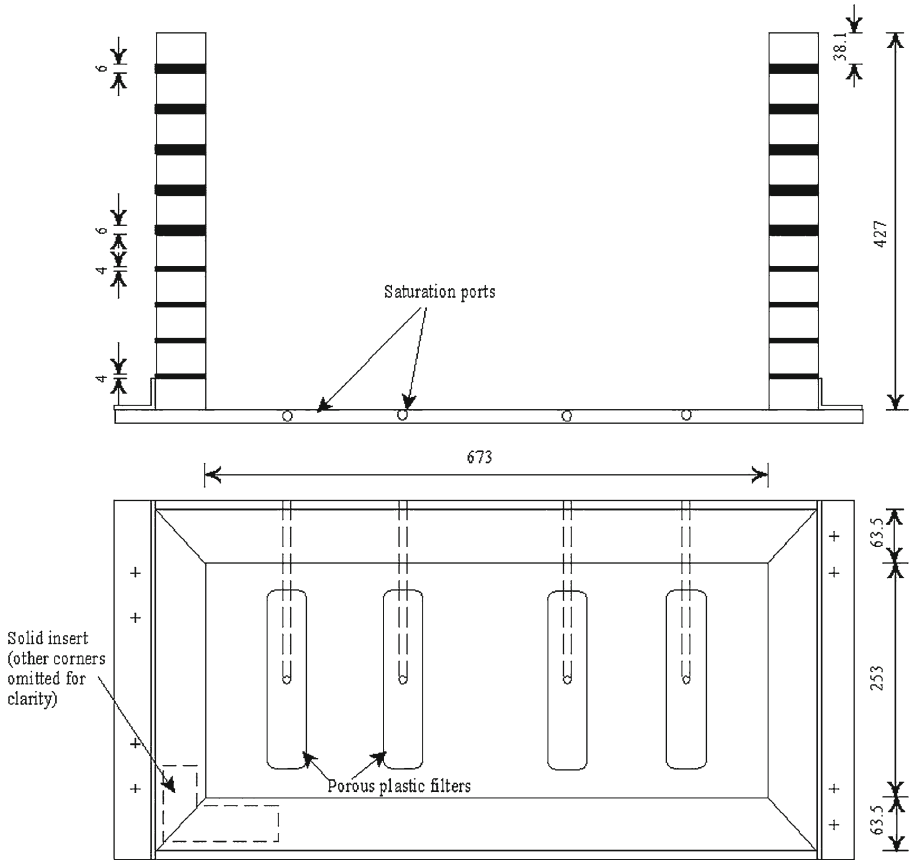

Fig. 7 Centrifuge container used in the tests at UCAM (Courtesy of UCAM)

during the strong shaking. The soil used in the tests was dry Hostun S28 sand. It was poured from a hopper inside the container, so that a void ratio of about 0.67 was achieved, filling it up to a height of 0.340 m. The SDOF structure was placed at the free surface of the soil.

The SDOF structure consists of two square plates of dimensions 0.1 by 0.1 by 0.00635 m for the structure and 0.1 by 0.1 by 0.00953 m for the foundation. Vertical walls of thickness 0.00163 m were constructed to connect the foundation with the structure. The total height of the structure is approximately 0.1 m (most accurately 0.0989 m). The total mass of the foundation-wall-structure system is 1.165 kg and the estimated bearing pressure of the soil about 57 kPa. From the 1.165 kg of the system mass, 0.525 kg is attributed to the structure and 0.64 kg to the foundation. Impulse testing of the structure showed that the fundamental frequency of the model structure is around 76–79 Hz.

Figure 8 shows the instrumented apparatus, with accelerometers in the soil and on the structure and displacement sensors on the free soil surface and on the top of the structure.

The centrifuge tests were performed at a 50 g environment, imposing a scaling by a factor of $N = 50$. The typical scaling factors are presented in Table 1, where M is the mass, L is the length, T is the time and N is the scaling factor depending on the environment. *Prototype* refers to the actual environment at the real site, while *Model* refers to the scaled, simulated environment in the centrifuge.

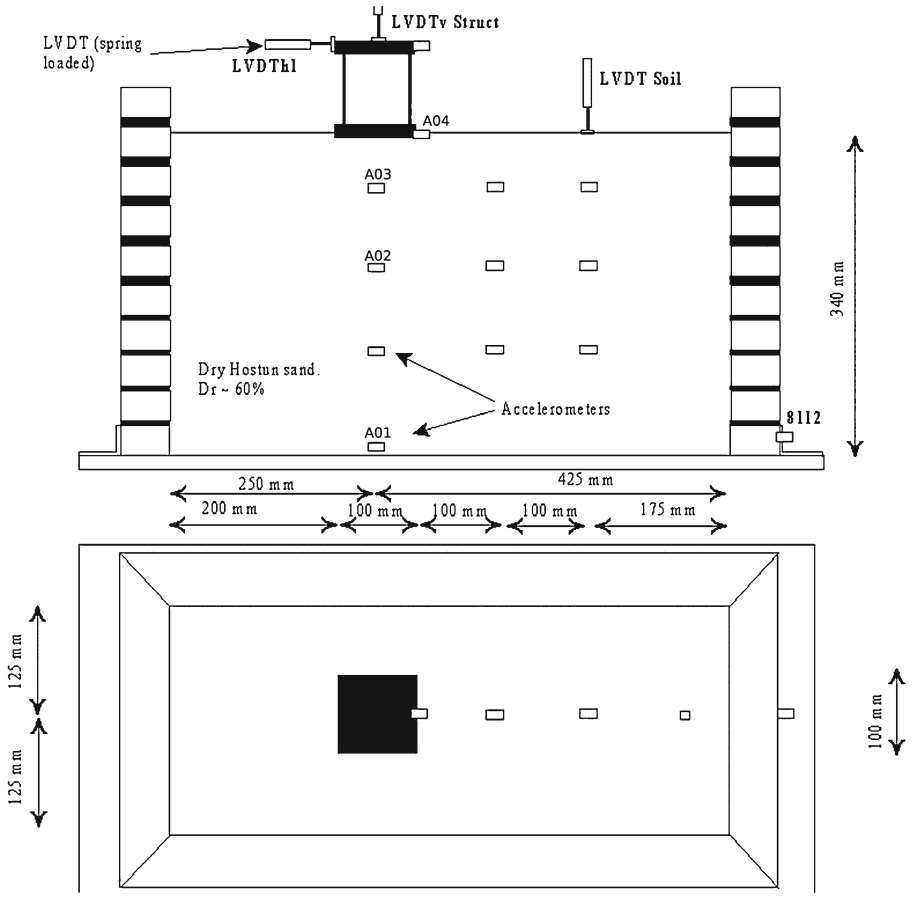

Fig. 8 Instrumented centrifuge apparatus used in the experiments in UCAM (Courtesy of UCAM)

Table 1 Centrifuge scaling factors

	Dimensions	Prototype	Model, N-g
Stress, pressure	$ML^{-1}T^{-2}$	1	1
Strain	–	1	1
Length, displacement	L	1	$1/N$
Velocity	LT^{-1}	1	1
Acceleration, gravity	LT^{-2}	1	N
Mass	M	1	$1/N^3$
Volume	L^3	1	$1/N^3$
Force	MLT^{-2}	1	$1/N^2$
Frequency	T^{-1}	1	N

The soil–foundation–structure configuration in the centrifuge was subjected to an artificial input motion with PGA = 18.55 g, duration 0.5 s and predominant frequency 50 Hz. After scaling to the *prototype conditions*, the response in the soil at the base of the container, recorded at the control point A01 (Fig. 8), is shown in Fig. 9. The earthquake ground motion

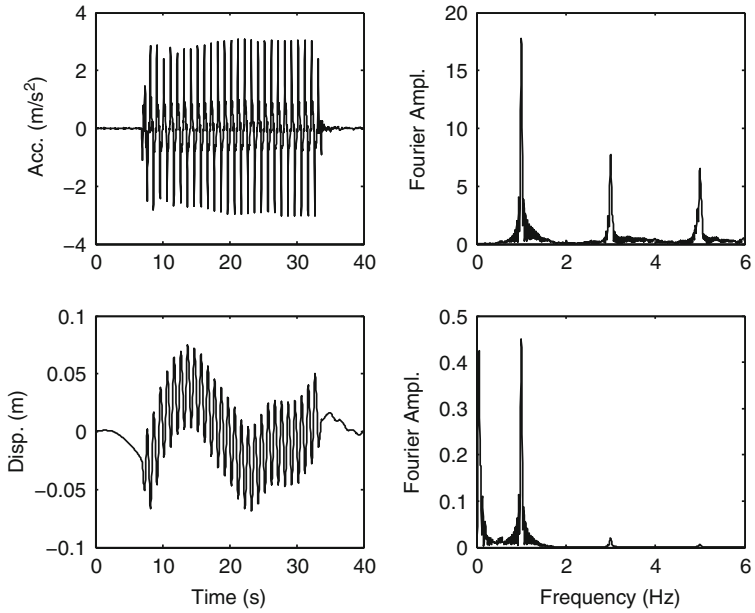

Fig. 9 Acceleration recording at the control point A01 (Fig. 8), after scaling to prototype conditions

induced in the centrifuge container was chosen to be strong enough, so that the nonlinear behavior of the soil is promoted.

3.2 Numerical modeling

The centrifuge testing was performed, as described in the preceding paragraph, in a 50 g environment, in order to simulate the prototype scale conditions in the centrifuge apparatus. To model the testing numerically, however, the prototype is chosen to be simulated in MISS3D-EqL.

The soil is modeled as a horizontal unbounded soil layer of total thickness $0.340 \cdot 50 = 17$ m, overlying a rigid bedrock. The shear wave velocity of the profile is calculated based on the following procedure: A depth of reference is chosen in the middle of the soil layer in the centrifuge container, at 0.170 m. This corresponds to a depth of $h_{\text{ref,prot}} = 0.170 \cdot 50 = 8.5$ m in prototype conditions. For a reference uniform unit weight $\gamma_{\text{ref,prot}} = 15\,\text{kN/m}^3$ in prototype conditions of the dry Hostun S28 sand, the total vertical stress at the depth of 8.5 m is:

$$\sigma_{\text{v,prot}} = \gamma_{\text{ref,prot}} \cdot h_{\text{ref,prot}} = 15 \cdot 8.5 = 127.5\,\text{kPa} \tag{44}$$

For a coefficient of lateral earth pressure at rest $K_{\text{o}} = 0.5$, the mean stress is in prototype conditions:

$$\sigma_{\text{o,ref,prot}} = \frac{(1 + 2K_o)\sigma_{\text{v,prot}}}{3} = 85\,\text{kPa} \tag{45}$$

For a void ratio $e = 0.67$, as imposed by the pouring of the sand inside the container, the reference shear modulus $G_{\text{ref,prot}}$ in prototype conditions is:

$$G_{\text{ref,prot}} = 3230\frac{(2.973 - e)^2}{1 + e}\sqrt{\sigma_{\text{o,ref,prot}}} = 81906\,\text{kPa} \tag{46}$$

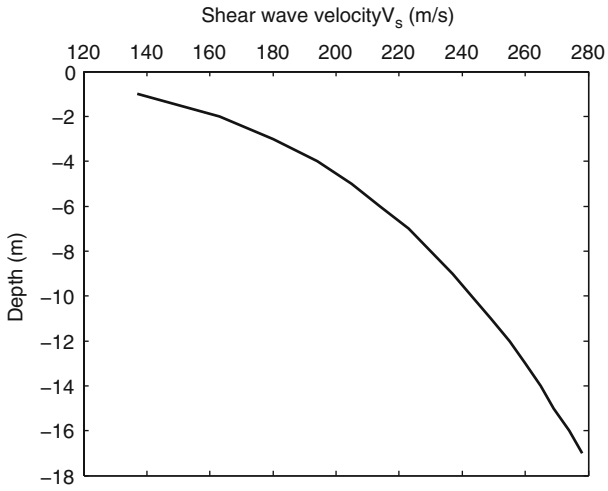

Fig. 10 Shear wave velocity profile in prototype conditions

In the centrifuge model conditions at a 50 g environment, the uniform unit weight of the dry Hostun S28 sand is $\gamma_{50g} = 1.5 \cdot 9.81 \cdot 50 = 735.75\,\text{kN/m}^3$. For a reference depth of $z_{\text{ref}} = 0.170\,\text{m}$ in the centrifuge container, the mean reference stress is

$$\sigma_{\text{o,ref,50g}} = \frac{(1 + 2K_{\text{o}})(\gamma_{50g} z_{\text{ref}})}{3} \tag{47}$$

and the mean stress at a depth z in the 50 g environment is

$$\sigma_{\text{o,50g}} = \frac{(1 + 2K_{o})(\gamma_{50g} z)}{3} \tag{48}$$

The shear modulus G_{50g} at a depth z will then be

$$G_{50g} = G_{\text{ref,prot}} \left(\frac{\sigma_{\text{o,50g}}}{\sigma_{o,ref,50g}} \right)^{0.5} \tag{49}$$

The shear wave velocity profile of the soil profile, in 50g environment, can then be calculated by the following equation

$$V_s = \sqrt{\frac{G_{50g}}{\rho}} \tag{50}$$

where $\rho = 1{,}500\,\text{kg/m}^3$ the uniform mass density of the dry Hostun S28 sand. As the scaling factor in the velocity in prototype conditions and in the 50g environment is 1:1, the shear wave velocity profile calculated by Eq. 50 in the 50 g environment can be applied in the prototype conditions as well. The shear wave profile that is introduced in MISS3D-EqL is shown in Fig. 10, calculated with the aforementioned procedure in prototype conditions. Control points are placed at the exact locations of the accelerometers set up in the centrifuge model.

In the soil, in order to take into account its nonlinear behavior, an equivalent linear approximation is pursued. Several shear modulus reduction and damping curves, commonly found in the literature (Kokusho 1980; Seed et al. 1986), were tested. After several analyses with varying form of the curves, the shear modulus reduction and damping curves that

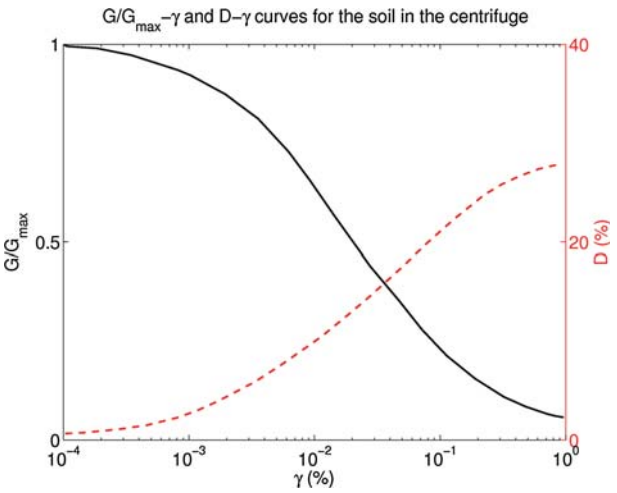

Fig. 11 Lower bound shear modulus reduction and upper bound damping curves for clean sands Seed et al. (1986), used in the MISS3D-EqL SFSI analysis with equivalent linear soil behavior

are found to best describe the nonlinear behavior of the soil are the curves of the lower bound shear modulus and upper bound damping curves for clean sands, proposed by Seed et al. (1986), and shown in Fig. 11. These curves are chosen based on the obtained soil response, compared to the recorded in the centrifuge. A linear elastic wave propagation analysis of the soil profile produces a fundamental frequency of the soil at approximately 3.7 Hz.

The structure is modeled as a SDOF oscillator with the mass lumped at the top. In the centrifuge model, the total mass of the structure is 1.165 kg, corresponding to the sum of the foundation and the structural mass. The total mass corresponds to a mass of 145,625 kg in prototype conditions. In the numerical analysis with MISS3D-EqL, however, the foundation is assumed to be massless. Thus, attributing the total mass of the foundation-structure system to the concentrated mass at the top of the structure causes the response to decline significantly from the recorded one. Consequently, only the 0.525 kg of the structural mass is considered in the numerical analysis. The 76–79 Hz of the natural frequency of the centrifuge SDOF structure correspond to a fundamental frequency of approximately 1.56 Hz in prototype conditions.

Figure 12 presents the calculated FRF connecting the control point at the base of the centrifuge container (control point A01 in Fig. 8) with the top of the structure. As the input motion shown in Fig. 9 has significant frequency content in the frequency range lower than 6 Hz, the recorded response is filterer above 6 Hz. The larger peak of the response is well captured by the equivalent linear model of MISS3D-EqL in terms of frequency and amplitude. This peak at about 1.47 Hz is attributed to the combined effects of the soil softening and the resonance of the structure. The difference between the linear and the equivalent linear approach is evidenced when plotting the calculated FRF between the top of the structure and the base of the container for purely linear soil behavior. The peak resonance frequency of the soil profile at 3.7 Hz for linear conditions, indicated as the second largest peak of the FRF in Fig. 12, shifts to lower frequencies (at 1.6 Hz) because of the equivalent linear soil behavior, with a significant decrease in the amplitude as well, due to energy dissipation. The resonance of the equivalent linear soil response at 1.6 Hz and the structural response produces

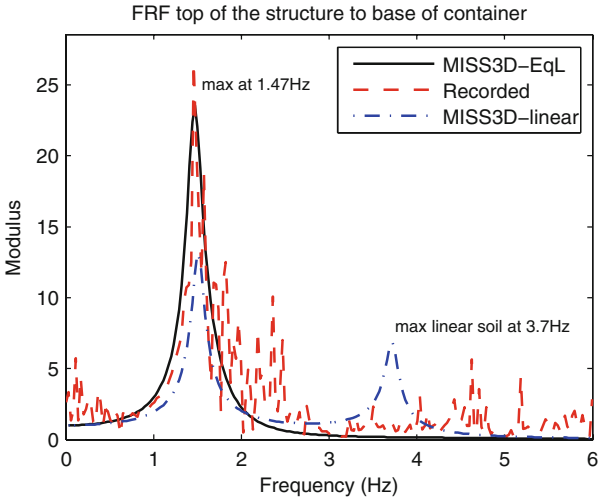

Fig. 12 Calculated (*solid line*) and recorded (*dashed line*) FRF relating the top of the structure with the control point A01, as well as FRF for purely linear elastic soil behavior (*dashed-dotted line*)

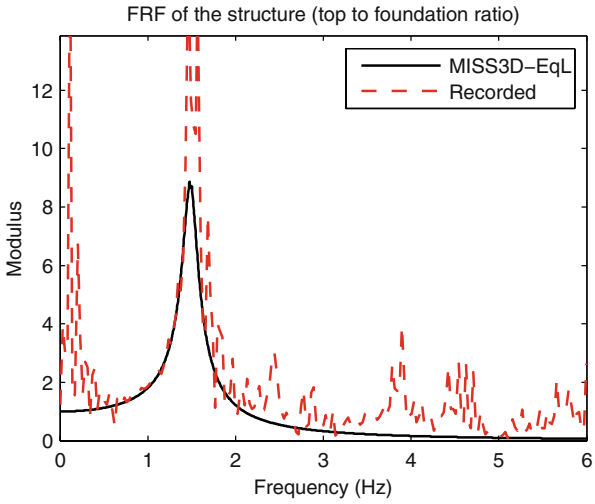

Fig. 13 Calculated (*solid line*) and recorded (*dashed line*) FRF relating the top of the structure with the foundation of the structure

the unique large peak at approximately 1.47 Hz, calculated with MISS3D-EqL and recorded in the centrifuge.

Figure 13 shows the FRF connecting the top of the structure with the side of the foundation. This would produce the FRF of the soil–foundation–structure system, resonating at a frequency lower than the fixed-base fundamental frequency of the structure at 1.56 Hz. Neglecting the random vibration noise in the recording, the system responds mainly in one frequency, at 1.47 Hz.

Figures 14, 15 and 16 show the comparison of the response calculated by MISS3D-EqL and the recorded response in the soil deposit, at the control points A01, A02 and A03, respectively shown in Fig. 8. The calculated response in the soil matches very well with the recorded response, in time and in frequency domain.

Figure 17 shows the response at the foundation. The recorded response is provided by the measurement of the accelerometer at the control point A04 (Fig. 8), while the response by MISS3D-EqL is calculated at the geometrical center of the foundation. Yet, the matching is

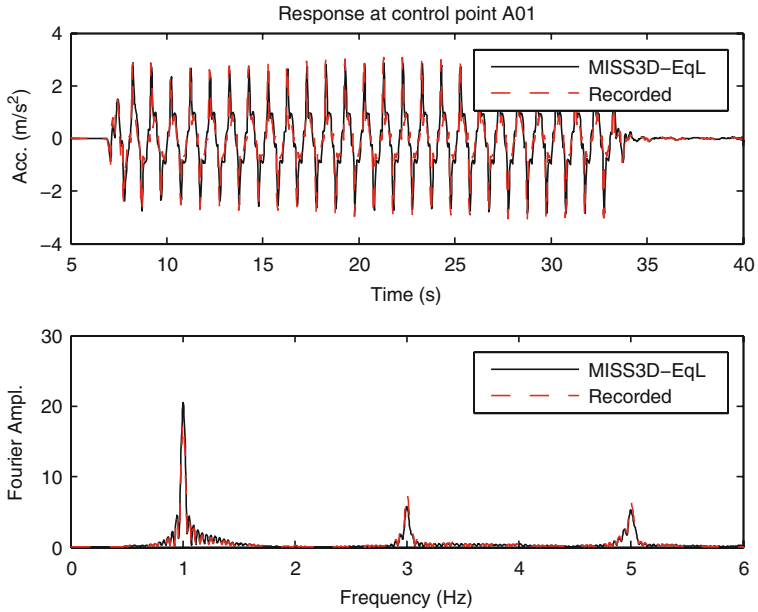

Fig. 14 Calculated (*solid line*) and recorded (*dashed line*) response at the control point A01

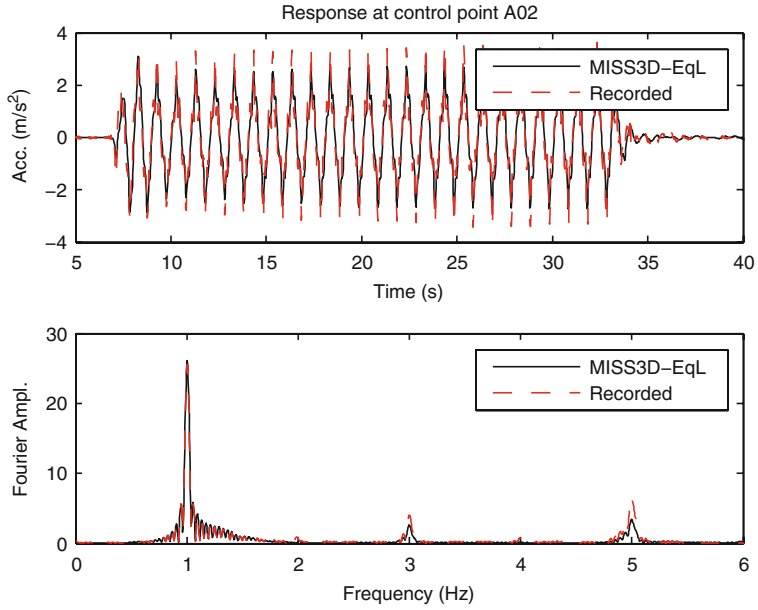

Fig. 15 Calculated (solid line) and recorded (dashed line) response at the control point A02

very good in the time and in the frequency domain, with minor differences arising from the inadequacy in capturing the resonance peak at 5 Hz, as shown at the bottom of Fig. 17.

In Fig. 18 is presented the comparison of the calculated and recorded response at the control point at the top of the structure. The structure responds in the frequency range between 0.9

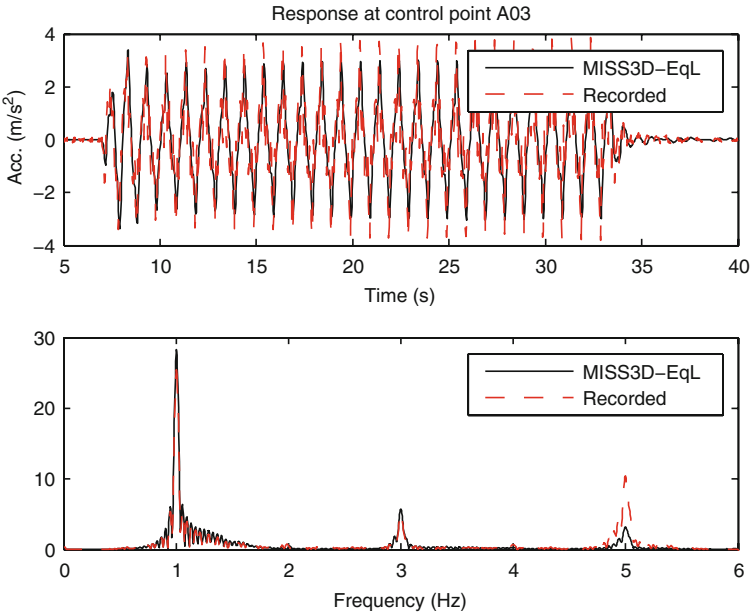

Fig. 16 Calculated (*solid line*) and recorded (*dashed line*) response at the control point A03

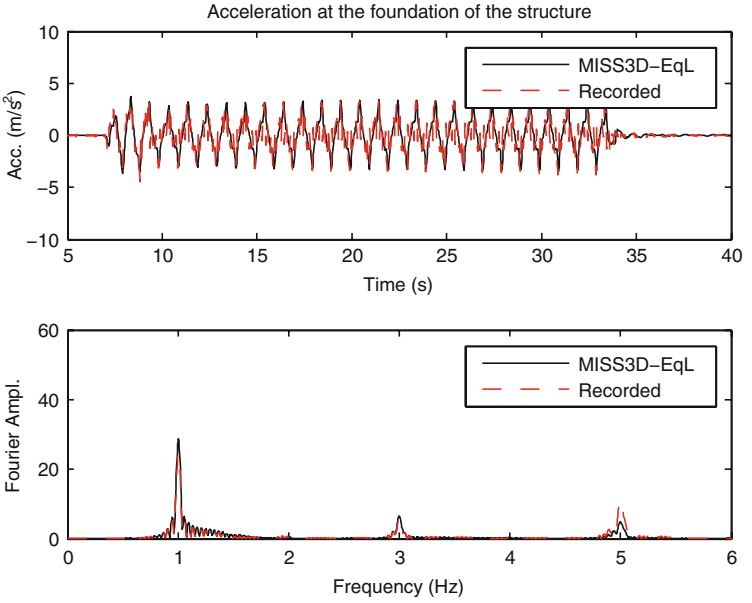

Fig. 17 Calculated (*solid line*) and recorded (*dashed line*) response at the foundation of the structure

and 2 Hz, as observed at the bottom of Fig. 18. The largest, sharp peak at 1 Hz is caused by the resonance with the input motion (Fig. 9, top right), while the resonance with the fundamental frequency of the structure takes place at around 1.47 Hz. The peak due to the resonance with

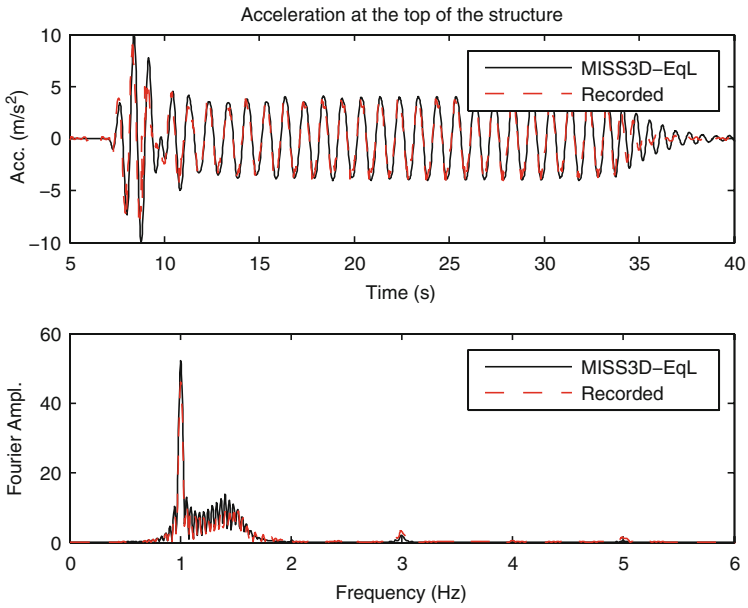

Fig. 18 Calculated (*solid line*) and recorded (*dashed line*) response at the top of the structure

the input signal is matched pretty well in amplitude. Minor difference exists though in the amplitude of the resonance peaks of the structure in the range of 1.1–1.6 Hz, the calculated response being larger. This minor difference in the amplitude of the response of the structure, in the frequency range between 1.1 and 1.6 Hz, is reflected in the time domain by the minor difference in amplitude in the time domain, in the fourth to the sixth peak, between 8 and 11 s. From the 11th second of the vibration and on, the system responds at the frequency of 1 Hz and the amplitude of the acceleration is essentially the same, proving that the equivalent linear substructure approximation is able to simulate efficiently the effects of the nonlinear soil behavior on the soil–foundation–structure system under a strong earthquake ground motion.

The difference between a linear and an equivalent linear approximation of the soil behavior in the SFSI analysis is demonstrated in Fig. 19. The acceleration of the structure is calculated with a linear soil model and an equivalent linear soil model, and then compared with the recorded response. A first observation would be that the amplitude assuming linear soil conditions is smaller than that for equivalent linear soil behavior. This difference is explained, however, by reexamining the FRF shown in Fig. 12. The effect of the soil softening, due to the approximation of the nonlinear behavior through an equivalent linear behavior, results in a shifting of the fundamental frequency of the soil response from approximately 3.7 Hz, in linear elastic conditions, down to around 1.6 Hz. The latter resonance of the equivalent linear soil, in conjunction with the resonance frequency of the structure at approximately 1.47 Hz (Fig. 13), creates large amplification of the response in the vicinity of 1.47 Hz. On the contrary, when a linear approximation is followed for the soil behavior, this coincidence of the resonant frequencies of the soil (3.7 Hz) and the structure (1.47 Hz) does not exist. Therefore, the amplitude of the response when an equivalent linear behavior is adopted for the soil is larger than the linear response. Nevertheless, the recorded response at the top of the structure is more efficiently captured assuming

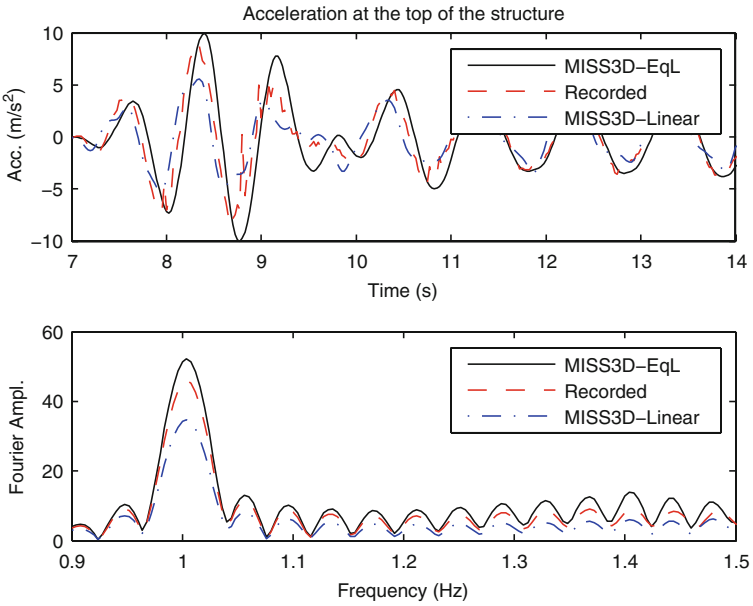

Fig. 19 Calculated (*solid line*) and recorded (*dashed line*) response at the top of the structure. The response of the equivalent linear analysis is compared with the linear soil response (*dashed-dotted line*) calculated with the linear MISS3D

equivalent linear soil behavior, enforcing the use of an equivalent linear soil model in the SFSI analysis.

4 Conclusion

A newly developed numerical procedure is presented and validated, introducing the equivalent linear soil behavior in the substructure approximation of the soil–foundation–structure interaction. The numerical code MISS3D performs SFSI analyses in the three-dimensional linear elastic or viscoelastic domain, based on the substructure method. MISS3D is extended in order to model the nonlinear soil behavior through an equivalent linear approach, resulting in a numerical tool named MISS3D-EqL. The key point of the proposed procedure is that the effect of the structural vibration on the soil response is taken into consideration at the same time as is the response of the soil to the incident wave field.

Moreover, based on the substructure method, the proposed procedure is strengthened by its simple formulation, providing physical insight and clarity in the phenomenon, while avoiding complexities arising from the FEM solution, such as the radiation condition to infinity. Furthermore, the aforementioned solution is easily implemented to account approximately, yet adequately, for the soil nonlinearity in the SFSI, with significantly lower computational cost.

Concluding, MISS3D-EqL is able to capture adequately the effects of both the primary and secondary nonlinear soil behavior. Effects of the primary nonlinearity, such as the soil softening and the larger energy dissipation, augmented by the secondary nonlinear effects due to the structural vibration, have impact on the response of the complete soil–foundation–structure system. The equivalent linear substructure approximation, however, is proved to

simulate efficiently the effects of the nonlinear soil behavior on the soil–foundation–structure system under a strong earthquake ground motion.

Acknowledgments This study was performed in the framework of the European research project entitled *New Methods for Mitigation of Seismic Rick of Existing Foundation (acronym (NEMISREF)*, EC contract No G1RD-CT-2002-00702, EC project No GRD1-2001-40457). The first author is in debt to Professor Arezou Modaressi of Ecole Centrale Paris, France, for her scientific coordination. The authors would like to thank Professor S. P. Gopal Madabhushi of University of Cambridge, UK and Dr. Andrew Brennan of the University of Dundee, Scotland, UK for providing the data of the centrifuge experiments and for their scientific expertise.

References

Aubry D, Clouteau D (1992) A subdomain approach to dynamic Soil–structure interaction. In: Recent advances in earthquake engineering and structural dynamics. Ouest Editions/AFPS, Nantes, France, pp 251–272

Bielak J (1975) Dynamic behavior of structures with embedded foundations. Earthq Eng Struct Dynam 3: 259–274. doi:10.1002/eqe.4290030305

Bode C, Hirschauer R, Savidis S (2002) Soil–structure interaction in the time domain using halfspace Green's functions. Soil Dyn Earthq Eng 22(4):283–295. doi:10.1016/S0267-7261(02)00020-9

Boore D, Stephens C, Joyner W (2002) Comments on baseline correction of digital strongmotion data: examples from the 1999 hector mine, california, earthquake. Bull Seismol Soc Am 92(4):1543–1560. doi:10.1785/0120000926

Brennan A, Madabhushi S (2002) Design and performance of a new deep model container for dynamic centrifuge testing. In: Proceedings of the international conference on physical modelling in geotechnics, Balkema, Rotterdam, The Netherlands, St Johns NF, Canada, pp 183–188

Chopra A (2001) Dynamics of structures. Prentice Hall Inc, Upper Saddle River

Clouteau D (2005) MISS 6.4: manuel utilisateur: version 2.3.. Chatenay-Malabry, France

Clouteau D, Aubry D (2003) Computational soil–structure interaction. In: Boundary element methods for soil–structure interaction, Kluwer Academic Publishers, chap. 2, pp 61–126

Gazetas G (1983) Analysis of machine foundation vibrations: state of the art. Soil Dyn Earthq Eng 2(1):2–42. doi:10.1016/0261-7277(83)90025-6

Gazetas G (1991) Formulas and charts for impedances of surface and embedded foundations. J Geotech Eng Div 117(9):1363–1381. doi:10.1061/(ASCE)0733-9410(1991)117:9(1363)

Ghosh B, Madabhushi S (2007) Centrifuge modelling of seismic soil structure interaction effects. Nucl Eng Des 237(8):887–896. doi:10.1016/j.nucengdes.2006.09.027

Halabian A, Naggar MHE (2002) Effect of non-linear soil-structure interaction on seismic response of tall slender structures. Soil Dyn Earthq Eng 22:639–658. doi:10.1016/S0267-7261(02)00061-1

Karabalis D (2004) Non-singular time domain BEM with applications to 3D inertial soil– structure interaction. Soil Dyn Earthq Eng 24(3):281–293. doi:10.1016/j.soildyn.2003.10.002

Kausel E, Roesset J, Christian J (1976) Nonlinear behavior in soil-structure interaction. J Geotech Eng Div 102(GT12):1159–1178

Kokusho T (1980) Cyclic triaxial test of dynamic soil properties for wide strain range. Soil Found 20(4):45–60

Madabhushi S, Schofield A, Lesley S (1998) A new stored angular momentum based earthquake actuator. In: Proceedings of centrifuge '98, Tokyo, pp 111–116

Mylonakis G, Nikolaou S, Gazetas G (2006) Footings under seismic loading: analysis and design issues with emphasis on bridge foundations. Soil Dyn Earthq Eng 26(9):824–853. doi:10.1016/j.soildyn.2005.12.005

Pitilakis D (2006) Soil–structure interaction modeling using equivalent linear soil behavior in the substructure method. Ph.D. thesis, LMSS-Mat, Ecole Centrale Paris, France

Pitilakis D, Dietz M, Wood DM, Clouteau D, Modaressi A (2008) Numerical simulation of dynamic soil-structure interaction in shaking table testing. Soil Dyn Earthq Eng 28(6):453–467. doi:10.1016/j.soildyn.2007.07.011

Roesset JM, Tassoulas JL (1982) Non linear soil-structure interaction: an overview. In: Datta SK (ed). Earthquake ground motion and its effects on structures, vol 53. ASME, AMD, Newyork, 59–76

Schofield A (1980) Cambridge geotechnical centrifuge operations. Twentieth rankine lecture. Geotechnique 30(3): 227–268

Schofield A (1981) Dynamics and earthquake geotechnical centrifuge modelling. In: Proceedings of the international conference on recent advances in geotechnical earthquake engineering and soil dynamics, University of Missouri-Rolla, Rolla, Missouri 3:1081–1100

Seed H, Wong R, Idriss I, Tokimatsu K (1986) Moduli and damping factors for dynamic analyses of cohesionless soil. J Geotech Eng 112(11):1016–1032. doi:10.1061/(ASCE)0733-9410(1986)112:11(1016)

Stewart J, Fenves G, Seed R (1999) Seismic soil–structure interaction in buildings i: analytical methods. J Geotech Geoenviron Eng 125(1):26–37. doi:10.1061/(ASCE)1090-0241(1999)125:1(26)

Veletsos A, Meek J (1974) Dynamic behavior of building-foundation systems. Earthq Eng Struct Dynam 3:121–138. doi:10.1002/eqe.4290030203

Veletsos A, Verbic B (1973) Vibration of viscoelastic foundations. Earthq Eng Struct Dynam 2:87–102. doi:10.1002/eqe.4290020108